Journal of Controlled Release 327 (2020) 186–197

Contents lists available at ScienceDirect

Journal of Controlled Release

journal homepage: www.elsevier.com/locate/jconrel

Optimizing the anti-tumor efficacy of protein-drug conjugates by engineering the molecular size and half-life

Fabian Brandl[a,b], Sarah Busslinger[a], Uwe Zangemeister-Wittke[a,b,*], Andreas Plückthun[a,*]

[a] Department of Biochemistry, University of Zurich, Winterthurerstrasse 190, CH-8057 Zurich, Switzerland
[b] Institute of Pharmacology, University of Bern, Inselspital INO-F, CH-3010 Bern, Switzerland

ARTICLE INFO

Keywords:
Tumor targeting
DARPin-drug conjugates
PASylation
XTENylation
Half-life extension

ABSTRACT

Despite some approvals of antibody-drug conjugates for cancer therapy, their clinical success rate is unsatisfactory because of very small therapeutic windows, influenced by on-target and off-target toxicities of conjugate and liberated toxin. Additional formats with systematically investigated molecular parameters must therefore be explored to increase their therapeutic window. Here we focused on the effective molecular weight. To generate conjugates with exactly defined drug loads and tunable pharmacokinetics, we used Designed Ankyrin Repeat Proteins (DARPins), fused to unstructured polypeptides of different lengths, to produce proteins with any desired half-life, to identify those with the best efficacy. We generated an EpCAM-targeting DARPin-MMAF conjugate, fused to PAS or XTEN of different lengths, and a matched series of controls of a non-binding DARPin to account for the enhanced permeability and retention (EPR) effect, covering half-lives of minutes to 20.6 h in mice. All conjugates were produced at high purity, and demonstrated high specificity and cytotoxicity in human tumor cell cultures, with IC_{50} values in the low nM range, independent of the polypeptide type and length. Due to their more facile purification, the PASylated conjugates were tested in nude mice bearing HT29 tumor xenografts. Independent of their size, all PASylated conjugates were very well tolerated after repeated systemic administration of 300 nmol/kg. We found that the conjugates with intermediate size and half-life showed the strongest anti-tumor effects, and deduced that this effect is a compromise of serum half-life and diffusion within the tumor, as on-rates and affinities are essentially identical, with extravasation playing only a very minor role.

1. Introduction

Tumor targeting with antibody-drug conjugates (ADCs) has emerged as a promising approach to more specific cancer therapy. By combining the specificity of a cell-binding domain with the destructive potential of a potent cytotoxin, the side-effects typically associated with conventional chemotherapeutics can be decreased [1]. Despite of research spanning several decades, only eight ADCs have been approved by the FDA (www.fda.gov) for the treatment of several malignancies, including relapsed acute myelogenous leukemia (AML), HER2-positive metastatic breast cancer, and relapsed or refractory diffuse large B-cell lymphoma (DLBCL). Numerous other ADCs are currently under preclinical and clinical investigation for various oncological indications and several candidates are expected to become approved soon [2].

Nonetheless, the key challenge in developing ADCs remains to find a therapeutic window, in other words, a suitable combination of efficacy and tolerable on-target and off-target toxicity of both the whole conjugate and the liberated toxin molecules. An important consideration is also their biodistribution and pharmacokinetics. Antibodies have limited potential to penetrate solid tumors and homogeneously distribute in the tissue [3], which consequently lowers efficacy and favors development of drug resistance. Antibodies have a very long half-life, but it is largely unknown what pharmacokinetic properties are needed to improve tumor localization and to maximize efficacy and tolerability.

For experiments designed to modulate the pharmacokinetic parameters and optimize the therapeutic window of drug conjugates by engineering, conventional ADCs with their intrinsically long serum half-life and — typically — heterogeneous drug-to-antibody ratios (DAR) are not ideal. Additionally, their bivalent nature, which might lead to unintended receptor activation especially after loss of the drug, is another challenge [4]. Finally, the development of safe and efficacious ADCs is thwarted by the molecular complexity of the IgG format, and the fact that the site of conjugation and drug-to-antibody ratios

* Corresponding authors at: Department of Biochemistry, University of Zurich, Winterthurerstrasse 190, CH-8057 Zurich, Switzerland.
E-mail addresses: uwe.zangemeister@pki.unibe.ch (U. Zangemeister-Wittke), plueckthun@bioc.uzh.ch (A. Plückthun).

https://doi.org/10.1016/j.jconrel.2020.08.004
Received 12 May 2020; Received in revised form 21 July 2020; Accepted 3 August 2020
Available online 06 August 2020

(DAR) will greatly affect aggregation propensity and stability, drug release and efficacy. This further complicates analysis, even though attempts to engineer functionally improved ADCs with increased site-specificity of drug conjugation and higher linker stability have been made [5].

The fundamental downsides of conventional ADCs have raised interest in alternative non-IgG binding scaffolds for the use in tumor targeting, such as Designed Ankyrin Repeat Proteins (DARPins), Adnectins, Affibodies and Kunitz domains, all of which are much better suited to optimally engineer the desired pharmacokinetic properties [6,7]. DARPins have been selected against a wide range of tumor markers using phage and ribosome display. Furthermore, they display favorable biophysical and biochemical properties with high thermodynamic stability, and can be expressed in the cytoplasm of *Escherichia coli (E. coli)* in high amounts, allowing cost-effective production at large scales [8]. The DARPin scaffold is by design devoid of internal cysteines and allows for extensive engineering, tolerating modifications at its N- and C-terminus [9]. A unique cysteine can be easily introduced at any place in the sequence, including the DARPins' C-terminus, for defined, site-specific drug conjugation, *e.g.*, for the facile generation of molecularly defined DARPin-drug conjugates with well-defined drug loads [10].

On the other hand, due to their small size and lack of FcRn recycling, DARPin-drug conjugates have very short serum half-lives of only a few minutes [10,11] and in unmodified form, they consequently suffer from poor tumor localization [12]. This limitation can in principle be overcome by conjugation to PEG [11], fusion to Fcγ or serum albumin [13,14], to albumin-binding proteins [15,16] or to unstructured half-life extension modules like PAS or XTEN [12,17,18]. On the other hand, longer circulation times might be assumed to decrease tolerability of drug conjugates due to off-target toxicity. Furthermore, as known from antibodies, large size inevitably impairs tissue penetration and hence anti-tumor efficacy [19,20]. Presumably, an optimal size exists for the two opposing effects: the benefit of increased tumor localization of cytotoxins due to longer persistence in the circulation *versus* the hindered diffusion of the whole drug conjugate in the tumor [21,22] and perhaps decreased tolerability.

To study these dependencies, and optimize tumor to non-tumor ratios and increase tumor penetration to optimize the therapeutic window, it is essential to have a very well-defined, controllable system. DARPins can be genetically fused to half-life extension modules of various lengths and site-specifically conjugated to cytotoxins in a facile manner [9,12]. They thus offer the opportunity to rigorously study the biochemical, pharmacokinetic, and therapeutic behavior as a function of molecular parameters.

Here we systematically investigated how apparent molecular size affects the tolerability and anti-tumor efficacy of a series of DARPin-cytotoxin conjugates (Ec1-MMAF), targeting the epithelial cell adhesion molecule (EpCAM) on solid tumors. Ec1-MMAF was produced with a defined drug-to-protein ratio of 1.0 and PASylated or XTENylated to different molecular sizes. A series of matching control molecules was produced which have no affinity for tumor cells, to account for the enhanced permeability and retention (EPR) effect of larger molecules. The efficacy and tolerability in tumor cell cultures and in tumor-bearing mice was systematically compared as a function of molecular parameters. We found that the anti-tumor effect was more pronounced for the medium size conjugates than for the largest one, and we examined explanations for this behavior.

2. Materials and methods

2.1. Construction of polypeptide-DARPin fusion proteins containing a single C-terminal cysteine for drug conjugation

The plasmid pQIq encoding the EpCAM-binding DARPin Ec1 [23] was modified (Fig. 1A) at the DARPin 5′-end by introducing a gene fragment encoding the superfolder green fluorescent protein (sfGFP) [24], followed by a Tobacco Etch Virus (TEV) cleavage site (ENLYFQG) and a FLAG-tag (DYKDDDDK) including a BmtI restriction site at the 3′-end. PAS (PAS300, PAS600, PAS900) and XTEN (XTEN288, XTEN576, XTEN864) sequences were introduced between the FLAG-tag and the DARPin by cloning via BmtI and BamHI restriction sites, as previously reported [12]. For site-specific conjugation of a cytotoxin to the fusion proteins, the 3′-end of the DARPin was exchanged with a gene fragment encoding a single cysteine within a GCG-motif in front of a TEV protease-cleavable His_6-tag (GCGENLYFQGHHHHHH). To generate non-binding fusion proteins as controls, DARPin Ec1 was replaced by DARPin Off7 [25], recognizing the *E. coli* maltose-binding protein. All constructs were expressed under the control of a T5 promoter (Fig. 1A).

2.2. Expression and purification of maleimide-reactive polypeptide-DARPin fusion proteins in large scale

All single-cysteine-containing DARPins and polypeptide-DARPin fusion proteins were expressed in *E. coli* BLR in ZYM-5052 [26] auto-induction media as previously reported [12]. After expression, the *E. coli* cells were pelleted by centrifugation at 4000 × *g* and washed by resuspension in PBS pH 7.4. For purification, cell pellets were re-suspended in 50 mM Tris-HCl pH 8.0, 400 mM NaCl (TBS400), supplemented with 3 mg/mL lysozyme, 100 μg/mL DNase I and lysed by sonication. Following sonication, lysates were centrifuged (21,000 × *g*, 30 min, 4 °C) and the supernatants were applied to a 500 mL Ni-NTA Superflow (Qiagen) metal affinity column connected to an Äkta Pure (GE Healthcare) FPLC system. The resin was washed with 50 mM Tris-HCl pH 8.0, 20 mM imidazole, in turn supplemented with 400 mM NaCl, 1 M NaCl or 20 mM NaCl, respectively, until the signal baseline at 280 nm was reached. After stringent washing, the proteins were eluted in PBS pH 7.4, 500 mM imidazole, collecting the eluate in fractions. Fractions containing the fusion proteins were pooled and applied to 25 mL GFP affinity-columns [27] and washed with each 15 CV of TBS400 and 15 CV TBS400 supplemented with 5 mM ATP, 5 mM $MgCl_2$. The GFP affinity-columns were equilibrated with 25 mM Tris-HCl pH 8.0, 300 mM NaCl, 0.5 mM EDTA, 1 mM DTT, and TEV protease (S219V mutant) [28], produced in-house, was added to a final concentration of 100 μg/mL. After incubation overnight at 4 °C, the cleaved proteins (with removed GFP- and His-tag) were eluted and concentrated by ultrafiltration (Amicon Centrifugal Filter Units, Millipore). Concentrated proteins were polished by preparative size exclusion chromatography on an Äkta Pure FPLC system (GE Healthcare) using a custom-made Superose 6 pg XK 16/60 (GE Healthcare) column and PBS pH 7.4, 300 mM NaCl, 5 mM DTT as running buffer. Fractions containing the desired proteins were pooled based on their UV traces and concentrated by ultrafiltration (Amicon Centrifugal Filter Units, Millipore).

2.3. Preparation of DARPin-MMAF and polypeptide-DARPin-MMAF conjugates

For site-specific conjugation of MMAF to the C-terminal cysteine of purified proteins, mcMMAF (HY-15578, MedChemExpress) was dissolved in anhydrous DMSO to a concentration of 5 mM. Protein samples were spiked with freshly dissolved DTT to a final concentration of 7.5 mM and reduced while shaking at 25 °C for 30 min. To remove DTT from the samples, the buffer was exchanged to rigorously degassed PBS pH 7.4, 1 mM EDTA on a HiPrep™ 26/10 Desalting column (GE Healthcare) connected to an Äkta Explorer (GE Healthcare) FPLC system. Desalted protein samples (15–30 μM) were mixed with a 2-fold molar excess of mcMMAF over reduced cysteine. For conjugation, the reaction was incubated for 4 h at 25 °C with shaking. The conjugation mixtures were then quenched by addition of a 5-fold molar excess of DTT over maleimide and incubated for 15 min at 25 °C with shaking. All steps were carried out under an argon atmosphere.

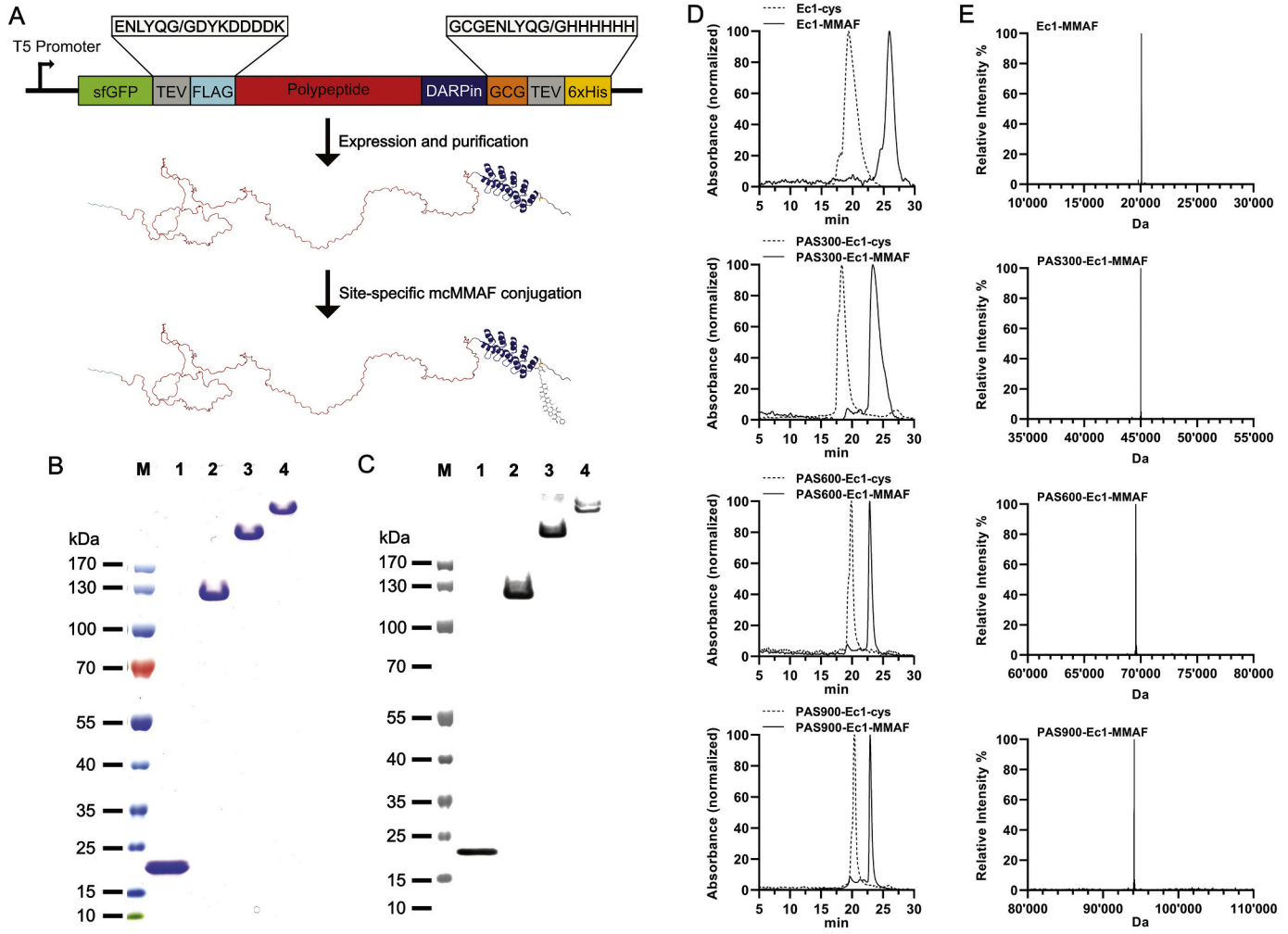

Fig. 1. Design and characterization of PASylated DARPin Ec1-MMAF conjugates. A) Schematic representation of expression constructs and a Rosetta-simulated exemplary model of a PAS300-DARPin-MMAF conjugate. B) SDS-PAGE of purified MMAF-conjugates, C) detection of the N-terminal FLAG-Tag by Western blotting with chemiluminescent immunodetection: lane 1) Ec1-MMAF, 2) PAS300-Ec1-MMAF, 3) PAS600-Ec1-MMAF, 4) PAS900-Ec1-MMAF. D) Analytical characterization of non-conjugated protein (dashed line) and purified protein-MMAF conjugates (filled line) by hydrophobic interaction chromatography. E) Analysis of purified protein-MMAF conjugates by ESI-MS, the values are shown in Table 1.

2.4. Small-scale purification of DARPin-MMAF and polypeptide-DARPin-MMAF conjugates for in vitro cell viability assays

For small-scale purification, DARPin-MMAF and polypeptide-DARPin-MMAF conjugates were purified by hydrophobic interaction chromatography (HIC). Briefly, a RESOURCE ISO (GE Healthcare) column was connected to an Äkta Micro FPLC system. Samples were diluted in 2× Buffer A (25 mM Na-phosphate pH 7.0, 2.7 M $(NH_4)_2SO_4$) to adjust the ammonium sulfate concentration to that in the running buffer A (25 mM Na-phosphate pH 7.0, 1.35 M $(NH_4)_2SO_4$). Samples with protein concentrations of 0.3 mg/mL were loaded onto the HIC column at a flow rate of 0.5 mL/min at 10 °C. Conjugates were eluted in a linear gradient of 5%B/min (Buffer B = 25 mM Na-phosphate pH 7.0). Fractions containing the conjugate were pooled and concentrated using Amicon Ultra Filter Tubes (Millipore). Purity was monitored by SDS-PAGE and analytical HIC, and was confirmed by ESI-MS.

2.5. Large-scale purification of DARPin-MMAF and PAS-DARPin-MMAF conjugates for in vivo tolerability and treatment studies

For large-scale purification of the MMAF conjugates from residual DTT, EDTA, quenched MMAF and other impurities, the conjugates were further polished by anion exchange chromatography. Briefly, conjugation mixtures were diluted 2-fold in 20 mM Tris-HCl pH 8.0 and were loaded onto a 1 mL Resource™ Q (GE Healthcare) anion exchange column connected to an Äkta Explorer (GE Healthcare) FPLC system running with Buffer A (20 mM Tris-HCl, 20 mM NaCl). Impurities were separated from the desired MMAF-conjugates by rigorous washing and stepwise elution with increasing percentage of Buffer B (20 mM Tris-HCl pH 8.0, 1 M NaCl). All steps were performed with a flow rate of 3–4 mL/min. Purity of samples was monitored by SDS-PAGE and analytical HIC, and was confirmed by ESI-MS.

2.6. Endotoxin removal

For endotoxin removal, purified proteins were applied to an EndoTrap HD (product discontinued, Hyglos GmbH) affinity resin according to the manufacturer's instructions. The buffer of eluted protein-MMAF conjugates was exchanged to endotoxin-free Dulbecco's PBS (Millipore) by PD-10 desalting columns (GE Healthcare). Endotoxin content was determined with an EndoSafe Portable Test System (Charles River Laboratories) using PTS test cartridges with 0.5–0.005 EU/mL sensitivity.

2.7. SDS-PAGE analysis

Equimolar amounts (113 pmol) of protein were analyzed by non-reducing SDS-PAGE using NuPAGE™ 4–12% Bis-Tris Protein Gels (Thermo Fisher Scientific) with NuPAGE™ MOPS SDS running buffer (Thermo Fisher Scientific). As molecular weight standard, PageRuler™ Prestained Protein Ladder (Fermentas) was used. Gels were stained with Coomassie Brilliant Blue R250 (Sigma-Aldrich).

2.8. Western blotting and immunodetection of the N-terminal FLAG-tag

For detection of the N-terminal FLAG-tag, 13 pmol of protein was separated on a NuPAGE™ 4–12% Bis-Tris Protein Gel (Thermo Fisher Scientific) and subsequently blotted to a Whatman™ 0.45 µm Protran Nitrocellulose membrane (Millipore) using a Trans-Blot® SD electrophoretic transfer cell (BioRad) and Towbin blotting buffer. The membrane was then blocked for 1 h with PBS-TB (PBS pH 7.4, 0.1% Tween-20, 5% w/v nonfat-dried milk) and washed three times with PBS-T (PBS pH 7.4, 0.1% Tween-20). Next, the membrane was incubated for 1 h with mouse anti-FLAG M2 primary antibody (Sigma-Aldrich, PN F3165) diluted 1:1000 in PBS-TM (PBS pH 7.4, 0.1% Tween-20, 0.5% w/v nonfat-dried milk). After washing three times with PBS-T, the membrane was incubated for 1 h with goat anti-mouse IgG H + L horseradish peroxidase conjugate (Thermo Fisher Scientific, PN 31438) diluted 1:5000 in PBS-TM. After stringently washing with PBS-T, PBS, and ddH_2O, SuperSignal® West Pico Chemiluminescent Substrate (Thermo Fisher Scientific, PN 34077) was prepared according to the manufacturer's instructions and chemiluminescence was measured using a Fusion FX spectra imaging device (Vilber). All steps were conducted at room temperature.

2.9. Analytical hydrophobic interaction chromatography

Purified conjugates were analyzed on a TSKgel Butyl-NPR (L × ID 3.5 cm × 4.6 mm, 2.5 µm particle size, Tosoh Bioscience) hydrophobic interaction chromatography column connected to a 1260 Infinity HPLC system (Agilent Technologies). Samples containing 8–16 µg protein conjugate were spiked with ammonium sulfate to a final concentration of 1.5 M $(NH_4)_2SO_4$ and loaded onto the column running with Buffer A (25 mM Na-phosphate pH 7.0, 1.5 M $(NH_4)_2SO_4$). For analysis, the proteins were eluted by a linear gradient of 33–83% Buffer B (25 mM Na-phosphate pH 7.0) in 50 min at a flow rate of 0.6 mL/min at 25 °C. UV absorbance was monitored at 280 nm and 230 nm. Data were analyzed using the OpenLab CDS ChemStation Edition Software (Version 1.3.4., Agilent Technologies).

2.10. Electrospray ionization mass spectrometry (ESI-MS)

Protein masses were determined by time-of-flight (TOF) ESI-MS at the Functional Genomics Center Zurich (FGCZ). Prior to ESI-MS analysis, samples were desalted by C4 ZipTip (Millipore, USA) reversed phase chromatography and eluted in MeOH:2-propanol:0.2% formic acid (30:20:50). The eluates were infused through a fused silica capillary (inner diameter 75 µm) at a flow rate of 1 µL/min and sprayed through a PicoTip with an inner diameter of 30 µm (New Objective, USA). Nano ESI-MS analysis of the samples was performed on a Synapt G2_Si mass spectrometer (Waters, UK) and the data were recorded with MassLynx 4.2. Software (Waters, UK). Mass spectra were acquired in positive-ion mode by scanning an *m/z* range from 100 to 5000 Da with a scan duration of 1 s and an interscan delay of 0.1 s. The spray voltage was set to 3 kV, the cone voltage to 40 V, and the source temperature to 80 °C. The recorded m/z data were then deconvoluted into mass spectra by applying the maximum entropy algorithm MaxEnt1 (MaxLynx) with a resolution of the output mass of 0.5 Da/channel and Uniform Gaussian Damage Model at the half height of 0.7 Da.

2.11. Analysis of the binding kinetics by surface plasmon resonance spectroscopy (SPR)

The binding kinetics of PASylated and XTENylated DARPin Ec1-MMAF conjugates and unfused Ec1-MMAF to the purified extracellular domain of human EpCAM (hEpEX) were determined on a ProteOn™ XPR36 instrument (BioRad). The ligand protein hEpEX was expressed, purified and enzymatically biotinylated as previously described [29]. First, two ligand channels of a NeutrAvidin-functionalized chip (ProteOn™ NLC Sensor Chip, BioRad) were coated with 500 RU of biotinylated hEpEX in PBS pH 7.4, 0.005% Tween 20, 3 mM EDTA. Following a buffer injection for baseline stabilization, a serial dilution of the polypeptide-DARPin fusion proteins (162 nM – 0.33 pM) was injected on separate ligand channels in duplicates. The flow rate of all steps was 60 µL/min, the association time and the dissociation time were 400 s and 2500 s, respectively. The chip surface coated with ligand was regenerated between analyte runs by two pulses of 25 µL 100 mM H_3PO_4 for 25 s. The sensorgrams were double-referenced by subtraction of interspot signals and a blank analyte channel. Data was fitted to a 1:1 Langmuir binding model and analyzed using the ProteOn™ Manager Software (Version 3.1.0.6, BioRad).

2.12. Cell lines and cell culture conditions

The EpCAM-positive human colon adenocarinoma cell line HT29 and the EpCAM-positive human breast adenocarcinoma cell line SKBR3 were obtained from DSMZ (German Collection of Microogranisms and Cell Cultures) and ATCC (American Type Culture Collection), respectively. The human embryonic kidney cell line HEK293T (ATCC) was used as EpCAM-negative control. HT29 and HEK293T cells were cultured in Dulbecco's Modified Eagle's medium (DMEM), SKBR3 cells were cultured in RPMI 1640 medium. All media were supplemented with 10% (v/v) heat-inactivated fetal calf serum (Amimed) and 1% (v/v) penicillin-streptomycin (Sigma-Aldrich). Cells were tested for human and murine pathogens (IDEXX BioResearch) and cultivated at 37 °C in a humidified atmosphere containing 5% CO_2.

2.13. Cell viability assay

The cytotoxicity of MMAF-conjugates against EpCAM-positive and -negative cells was tested in colorimetric XTT cell proliferation assays (BioFroxx, PN 1167TT000). Cells were grown to a confluency of 80–90%, trypsinized and diluted in fresh medium. Cell counts were determined with a CASY®TT cell counter and seeded into 96-well cell culture plates at a density of 5000 cells per well in 100 µL of medium, and grown for 24 h at 37 °C, 5% CO_2. The medium was then replaced by dilution series of the protein-MMAF conjugates or free MMAF in 50 µL culture medium. To normalize the response, cells treated with 5 mg/mL hygromycin B were used as positive control, non-treated cells were used as negative control. All conditions were analyzed in triplicates. After 72 h, the medium was aspirated and replaced by 50 µL of XTT reagent prepared according to the manufacturer's instructions, and with 50 µL fresh medium. After incubation for 1–2.5 h at 37 °C, 5% CO_2, UV absorbance was measured at 463 nm and 670 nm reference wavelength with an Infinite® M1000 plate reader (Tecan). Dose-response curves with variable slopes were fitted to all data points with the equation ($y = y_{min} + ((y_{max}-y_{min})/(1 + 10^{(\log(IC50)-x)\cdot HillSlope})$) using the GraphPad Prism software (Version 8.1.2. (441)), where y is the normalized absorption, x is the drug conjugate concentration, y_{min} and y_{max} are the bottom and top plateau. The IC_{50} value is the concentration of drug at which cell viability was decreased by 50%.

2.14. Mice

Female Crl:CD1-*Foxn1*^{nu} mice were purchased from Charles River Laboratories and housed under sterile conditions according to the

guidelines of the veterinary ordinance of the Kanton of Zurich (Switzerland) for animal welfare.

2.15. Tolerability study

To identify which doses and which dosing schedules are tolerated and safe, Crl:CD1-*Foxn1*^{nu} mice ($N = 3$ per construct, 7 weeks of age) were injected into the tail vein with 200 nmol/kg and 300 nmol/kg MMAF, Ec1-MMAF, PAS300-Ec1-MMAF, PAS600-Ec1-MMAF, PAS900-Ec1-MMAF, and PBS every other day for five times. The body weight of the mice was monitored daily. One week after the last injection, mice were sacrificed and blood was collected by heart puncture. Blood was analyzed for blood cell counts of thrombocytes, leukocytes, erythrocytes, and levels of creatinine, total bilirubin, and aspartate aminotransferase (ASAT) and alanine aminotransferase (ALAT) activity in the blood were determined. All analyses were performed at the Veterinary Medical Laboratory of the University of Zurich according to IFCC (International Federation of Clinical Chemistry and Laboratory Medicine) standards. Data analysis was performed using the GraphPrism 8 software package (Version 8.1.2. (441)). Safe dosing was determined as dosing where the body weight did not reduce more than 15% relative to the body weight at the day of the first injection, and blood counts, creatinine, bilirubin, ASAT and ALAT levels did not exceed critical levels.

2.16. Anti-tumor efficacy

Tumor xenografts were grown on the back of Crl:CD1-*Foxn1*^{nu} mice aged 6 to 7 weeks by subcutanous injection of 8×10^6 HT29 cells, and anti-tumor efficacy was determined when tumors reached an average volume of 100 mm^3. Tumor measurement was done double-blinded and mice were allocated into treatment groups with 6 mice each. All treatment groups were injected into the tail vein every other day for five times with 300 nmol/kg of MMAF, Ec1-MMAF, PAS300-Ec1-MMAF, PAS600-Ec1-MMAF, PAS900-Ec1-MMAF, Off7-MMAF, PAS300-Off7-MMAF, PAS600-Off7-MMAF, PAS900-Off7-MMAF in 150 μL PBS, or for untreated controls with 150 μL PBS. The body weight of mice was monitored daily by weighing and tumor size was measured with a digital caliper. The tumor volume was calculated with the formula: (short diameter)^2 × (long diameter) × 0.4. Euthanasia criteria were defined as body weight loss of more than 15% relative to the body weight at treatment start or as tumor size larger than 1000 mm^3. After termination of treatment, body weight and tumor size were monitored three times per week for another 40 days.

2.17. Statistical analysis of anti-tumor efficacy

The one-way analysis of variance (ANOVA) test for multiple comparisons was performed using the GraphPrism 8 software package (Version 8.1.2. (441)). For comparison, the mean tumor volume on day 18 after treatment start was chosen. The sigificance level was defined as $P < 0.05$.

3. Results

We recently reported the fusion of PAS and XTEN polypeptides of various lengths to the EpCAM-targeting DARPin Ec1 and the control DARPin Off7 [12]. The polypeptides were produced with pairs of comparable lengths ranging from short (XTEN288 / PAS300), over intermediate (XTEN576 / PAS600) to very long (XTEN864 / PAS900) polypeptide sequences. The number refers to the amino acid residues (the PAS300 polypeptide, *e.g.*, consists of 300 amino acid residues). Thereby, the hydrodynamic radii of the fusion proteins strongly increased, extending the serum half-life of the unmodified DARPins in mice stepwise from 11 min up to 20.6 h, depending on the polypeptide length and type. Although the polypeptides (PAS and XTEN) showed the same pattern of organ distribution in mice, their localization to EpCAM-positive tumors was target-specific and correlated with molecular size.

3.1. Construction of generic polypeptide-DARPin fusion proteins and DARPins with single cysteines for site-specific drug conjugation

To elucidate the relationship between a therapeutic protein's *in vivo* serum half-life, tolerability and efficacy, a unique cysteine was introduced at the DARPins' C-terminus for conjugation. To this end, a segment 3′ of the DARPin was exchanged with a DNA fragment encoding a Gly-Cys-Gly (GCG) motif, followed by a TEV cleavage site and a hexahistidine-tag (GCGENLYFQG/GGSHHHHHH) (Fig. 1A). This allowed the site-specific and defined addition of a single cytotoxin (maleimidocaproyl monomethyl auristatin F - mcMMAF [30]) to the proteins by maleimide-thiol conjugation (Fig. S1).

3.2. Production of DARPins and polypeptide-DARPin fusions containing single cysteines for site-specific mcMMAF conjugation

All DARPins and polypeptide-DARPin fusion proteins with a unique C-terminal cysteine were expressed in *E. coli* and purified using a protocol adapted from that recently reported [12]. After a four-step purification procedure, the proteins were highly pure and exhibited native biochemical and biophysical properties (Fig. S2, Fig. S3). Since the presence of His-tags on proteins can lead to increased liver accumulation in mice [31,32], the polyhistidine-tags (His_6-Tag) (Fig. 1A) on the proteins, used for purification by IMAC, were removed during the purification procedure by TEV cleavage. Successful removal of the polyhistidine-tags from the proteins was analyzed by Western blotting of purified proteins and immunodetection of His-tags. This showed the absence of any band except for the uncleaved controls (Fig. S4), confirming the successful removal and depletion of any His-tag containing protein. Detection of the N-terminal FLAG-tag on Western blots confirmed the prescence of only full-length proteins without any signs of degradation (Fig. S5).

3.3. Preparation and characterization of highly pure and molecularly defined DARPin-MMAF and polypeptide-DARPin-MMAF conjugates

For conjugating purified DARPins and polypeptide-DARPin fusions with a cytotoxin, maleimidocaproyl-functionalized monomethyl auristatin F (mcMMAF) was conjugated to the unique cysteine introduced at the DARPins' C-terminus. The presence of mcMMAF in the proteins increased the hydrophobicity, incremented by the prescence of the caproyl linker, and it added an additional charge by the C-terminal carboxyl group of MMAF to the conjugates. Therefore, hydrophobic interaction chormatography (HIC) was used to purify MMAF conjugates on small scales (5–10 mg) for initial characterization and comparison of PASylated and XTENylated DARPin-MMAF conjugates in cell viability assays (XTT). Larger amounts (70–100 mg) for *in vivo* tolerability and treatment studies of PAS-DARPin-MMAF conjugates were purified by anion exchange chromatography (AEX). Both strategies, HIC and AEX, led to highly pure conjugate preparations (Fig. 1B,C,D,E, Fig. S6, S7). SDS-PAGE and Western blotting with N-terminal FLAG-tag detection confirmed the purity and integrity of the protein-MMAF conjugates (Fig. 1B,C, Fig. S6). Analytical HIC (Fig. 1D, Fig. S7) showed that all samples were mono-conjugated with drug-to-protein ratios (DPR) of 1.0 and purities of > 95% (Table 1, Table S1) for all purified conjugates, and electrospray ionization mass spectroscopy (ESI-MS) (Fig. 1E, Fig. S7) confirmed the correct masses.

To investigate the effect of C-terminal conjugation of mcMMAF to the DARPins and polypeptide-DARPin fusion proteins on EpCAM binding, binding kinetics were determined by surface plasmon resonance measurements (SPR). Previous experiments showed that the fusion of PAS and XTEN polypeptides to the DARPins' N-terminus

Table 1
Biophysical characterization of PASylated and unmodified EpCAM-targeting DARPin Ec1.

Construct	MW_{calc}[a] (kDa)	MW_{exp_MS}[b] (kDa)	Purity[c] (%)	k_a[d] (M^{-1} s^{-1})	k_d[d] (s^{-1})	K_D[d] (M)
Ec1-MMAF	20.083	20.083	> 95%	2.14×10^5	1.39×10^{-5}	6.48×10^{-11}
PAS300-Ec1-MMAF	45.007	45.007	> 95%	5.80×10^4	8.41×10^{-6}	1.41×10^{-10}
PAS600-Ec1-MMAF	69.571	69.571	> 95%	4.11×10^4	1.08×10^{-5}	2.62×10^{-10}
PAS900-Ec1-MMAF	94.136	94.136	> 95%	3.83×10^4	8.41×10^{-6}	2.19×10^{-10}

[a] Molecular weights were calculated (MW_{calc}) with the ProtParam tool on the ExPASy server, based on the amino acid sequence of the polypeptide-DARPin fusion constructs.
[b] Experimental molecular weights (MW_{exp_MS}) were determined by ESI-MS (*cf.* Fig. 1E).
[c] Purity was determined by analytical hydrophobic interaction chromatography on an HPLC system (*cf.* Fig. 1D). The purity is indicated as percentage and corresponds to the integrated conjugate peak area.
[d] Binding kinetics to EpCAM (hEpEx) were determined by surface plasmon resonance (SPR, *cf.* Fig. S8).

altered the apparent equilibrium dissociation constant (K_D) of DARPin Ec1 for EpCAM by slightly decreasing the association rate constant (k_a), while keeping the dissociation rate constant (k_d) unaltered [12]. As expected, SPR measurements showed that MMAF conjugation to the fusion proteins altered the association and dissociation rates only marginally within the error of the measurements and thus did not affect the equilibrium dissociation rates (K_D) (Table 1, Table S1, Fig. S8); therefore, these binding kinetics equal those previously reported for non-conjugated polypeptide-DARPin fusion proteins [12].

3.4. Cytotoxicity of the polypeptide-MMAF conjugates in cell viability assays

On EpCAM-positive cells, all conjugates with DARPin Ec1 were more cytotoxic than the corresponding non-binding control conjugates with DARPin Off7, typically by about 3 orders of magnitude, regardless of the type of polypeptide used for fusion (Fig. 2, Table 2, Fig. S9, Table S2). In contrast to their effects on EpCAM-positive cells, EpCAM-targeting and non-targeting conjugates did not show measurable differences in cytotoxicity against EpCAM-negative HEK293T cells. Compared to unmodified Ec1-MMAF (HT29: IC_{50} = 1.7 nM, SKBR3: IC_{50} = 0.07 nM), the polypeptide-Ec1-MMAF conjugates showed in general somewhat higher IC_{50} values on HT29 cells (IC_{50} = 6.3 nM – 15.4 nM) and SKBR3 cells (IC_{50} = 0.9 nM – 4.8 nM) (Fig. 2, Table 2, Fig. S9, Table S2), and for the XTENylated conjugates this effect tended to slightly increase with the length (Fig. S9, Table S2). Nonetheless, the IC_{50} values for all polypeptide-Ec1-MMAF conjugates were very similar, and no correlation between cytotoxicity and polypeptide type could be found, indicating that PASylated and XTENylated DARPin-MMAF conjugates are equally potent. Furthermore, as shown for the PASylated conjugates, the differences in EpCAM-binding kinetics due to different polymer length (Fig. S8, Table S1) did not substantially affect the kinetics of intoxication, *i.e.,* the time dependence of the XTT assay, and only marginally decreased potency (Fig. S10).

3.5. Tolerability of PASylated DARPin-MMAF conjugates

To investigate the relationship of very short (DARPin), short (PAS300-DARPin), intermediate (PAS600-DARPin) and long (PA900-DARPin) serum half-lives and tolerability of the conjugates with identical specificity and drug-to-protein ratio, nude mice were injected with increasing equimolar doses of conjugate, using the same injection schedule as for the treatment studies in tumor-bearing mice. To this end, mice (groups of 3 per construct and dose) were injected i.v. every other day for five times with 200 nmol/kg and 300 nmol/kg of the conjugates, and the body weight was monitored daily. One week after the last injection, aspartate aminotransferase (ASAT), alanine aminotransferase (ALAT), creatinine and total bilirubin levels, as well as blood cell counts (erythrocytes, thrombocytes, leukocytes) were measured and compared to PBS-injected mice, and abnormal levels were used to assess toxicity. This dose-finding experiment provided a window of well-tolerated doses, which were later used in the treatment study.

Daily monitoring of body weight and blood analysis after euthanasia indicated that both doses, 200 nmol/kg and 300 nmol/kg, were well tolerated. During the treatment for 10 days, the body weight did not decrease by more than 5% relative to the day of the first injection. ASAT, ALAT, creatinine and total bilirubin levels, as well as blood cell counts were within the expected range and comparable to the levels in PBS-injected mice (Fig. 3, Fig. S11). All measured parameters were also comparable with the reference levels of North American CD-1 nude mouse colonies reported by Charles River International (www.criver.com / CD-1 Nude Mouse Hematology and Biochemistry). In summary, this indicates that for all tested conjugates, doses of 200 nmol/kg and 300 nmol/kg given every other day for five times were well tolerated.

3.6. Anti-tumor efficacy of PASylated DARPin-MMAF conjugates

The effect of molecular size and half-life on the anti-tumor efficacy was investigated in nude mice bearing EpCAM-positive HT29 tumor xenografts using the PASylated DARPin-MMAF conjugates of different length at the well tolerated doses and injection schedule described above. Control mice received PBS, free MMAF or the non-targeting conjugates Off7-MMAF, PAS300-Off7-MMAF, PAS600-Off7-MMAF and PAS900-Off7-MMAF.

As expected, despite its high potency *in vitro*, no anti-tumor effect was seen with free MMAF and with the small DARPin Ec1-MMAF conjugate (Fig. 4A,B, Fig. S12). In contrast, with the EpCAM-targeting PASylated conjugates, pronounced anti-tumor effects were measured with PAS300-Ec1-MMAF and PAS600-Ec1-MMAF. Tumors started to rapidly shrink after the third injection and were hardly measurable at day 10 to 15 after the start of treatment when differences among the treatment groups were greatest. Thereafter, tumors regrew to an average volume of 100 mm^3 on day 20 (Fig. 4A,C, Fig. S12). In both treatment groups, one out of six mice showed complete tumor regression. The strong anti-tumor effect of PAS300-Ec1-MMAF and PAS600-Ec1-MMAF is mirrored by an estimated overall survival of 33% at day 50 (Fig. 4B).

Surprisingly, PAS900-Ec1-MMAF, the construct with the largest molecular size and longest serum half-life, was clearly less effective, and tumor growth could be controlled only during the first 10 days of treatment (Fig. 4A,C, Fig. S12). This difference in efficacy cannot be explained by delayed intoxication of the cells (Fig. S10).

None of the non-targeting control conjugates (Off7-MMAF, PAS300-Off7-MMAF, PAS600-Off7-MMAF, PAS900-Off7-MMAF) inhibited tumor growth when compared to PBS (Fig. 4A,C, Fig. S12). The highly significant difference ($P < 0.0001$) in efficacy of the various size-matched targeting and non-targeting conjugates reflects the window of specificity which can be reached with the treatments (Fig. 4C, Fig. S13). This demonstrates that designed modulation of molecular size and serum half-life is crucial to find the most effective drug conjugate for tumor targeting in a defined preclinical setting. It also allows us to draw some conclusions about the origins of this effect to guide the

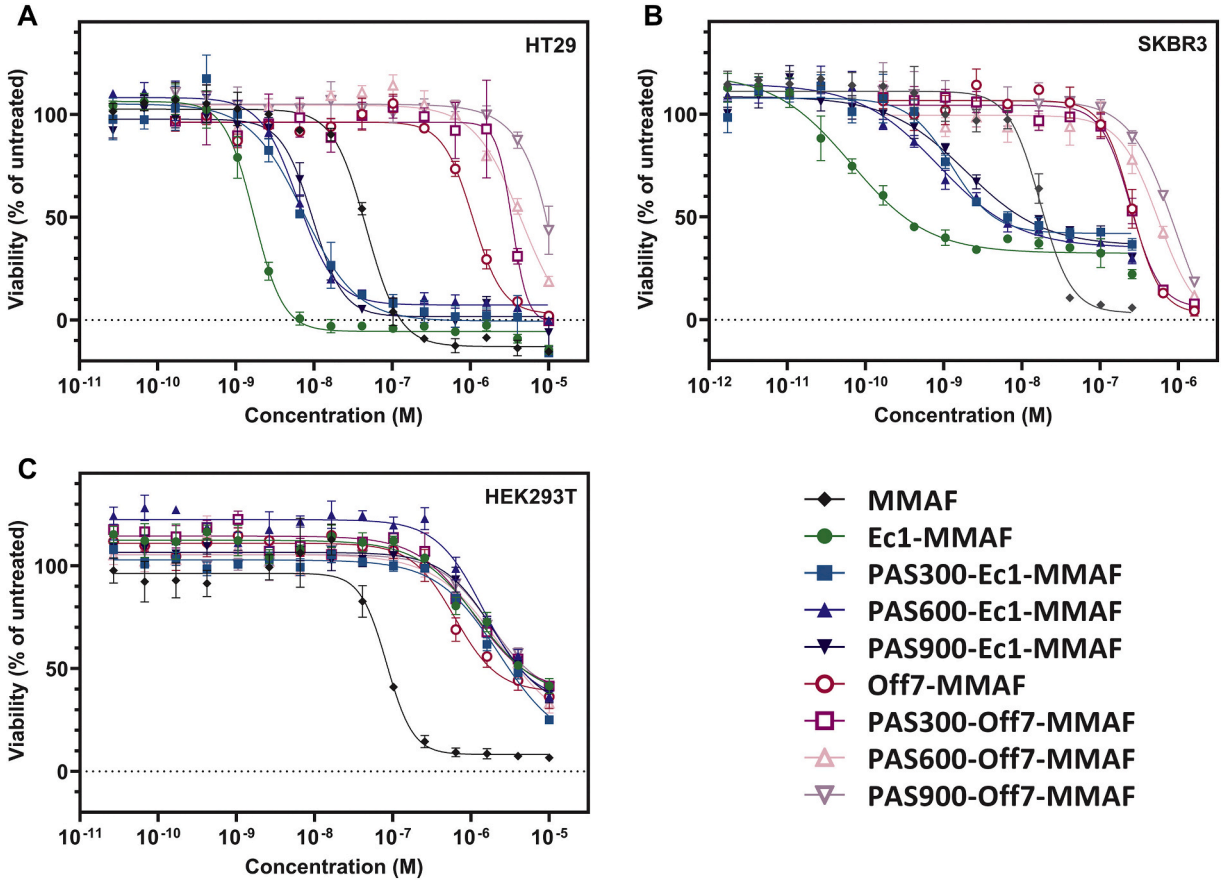

Fig. 2. Cytotoxicity of DARPin-MMAF and PAS-DARPin-MMAF conjugates determined in XTT cell viability assays. The EpCAM-specific conjugates Ec1-MMAF and PAS-Ec1-MMAF were compared to the control conjugates Off7-MMAF, PAS-Off7-MMAF, and to free MMAF. EpCAM-positive cell lines were A) HT29 and B) SKBR3, in C) EpCAM-negative HEK293T cells were used as control. Cells were incubated with a serial dilution of the MMAF conjugates and free MMAF for 72 h before cytotoxicity was determined. Each data point corresponds to the mean of triplicate measurements ± SD.

Table 2
Cytotoxicity[a] of MMAF, DARPin-MMAF and PAS-DARPin-MMAF conjugates.

Conjugate	HT29 IC_{50}[b] (M)	SKBR3 IC_{50}[c] (M)	HEK293T IC_{50}[d] (M)
MMAF	4.65×10^{-08}	1.70×10^{-08}	8.36×10^{-08}
Ec1-MMAF	1.70×10^{-09}	6.54×10^{-11}	1.23×10^{-06}
PAS300-Ec1-MMAF	7.27×10^{-09}	1.26×10^{-09}	2.27×10^{-06}
PAS600-Ec1-MMAF	6.27×10^{-09}	8.64×10^{-10}	1.46×10^{-06}
PAS900-Ec1-MMAF	9.54×10^{-09}	1.91×10^{-09}	1.96×10^{-06}
Off7-MMAF	1.07×10^{-06}	2.52×10^{-07}	6.21×10^{-07}
PAS300-Off7-MMAF	3.41×10^{-06}	2.46×10^{-07}	1.08×10^{-06}
PAS600-Off7-MMAF	4.49×10^{-06}	5.55×10^{-07}	2.30×10^{-06}
PAS900-Off7-MMAF	1.63×10^{-04}	9.48×10^{-07}	1.80×10^{-06}

[a] cytotoxicity was determined in XTT cell viability assays (IC_{50}: concentration at which cell viability was decreased by 50%).
[b] HT29 is an EpCAM-positive cell line.
[c] SKBR3 is an EpCAM-positive cell line.
[d] HEK293T is an EpCAM-negative control cell line.

development of optimal targeted conjugates.

4. Discussion

Antibody-drug conjugates (ADCs) have demonstrated improved therapeutic potential compared to standard chemotherapy, but clinical success rates are still far from satisfactory. To obtain acceptable therapeutic windows, many interdependent molecular parameters have to be optimized at the same time. One of them is molecular size, as it influences pharmacokinetics and tissue distribution, and thus impacts on both efficacy and tolerability. Unfortunately, it would be difficult to systematically investigate this with conventional ADCs, especially if there is an additional complication from the range of drug-to-antibody ratios in the preparation, as opposed to molecularly defined species. Therefore, it has remained largely unknown how the optimal conjugate should be engineered with regard to molecular size and pharmacokinetics.

Here, we generated EpCAM-targeting DARPin-MMAF conjugates as fusions with the unstructured polypeptides PAS or XTEN at different lengths to stepwise modify their size and hence serum half-life from 11 min to 20.6 h in mice. Cytotoxicity, specificity, anti-tumor efficacy, and tolerability were investigated in preclinical models with human tumor cell lines *in vitro* and *in vivo*.

4.1. Polypeptide-DARPin-MMAF conjugates can be produced as molecularly defined preparations

Site-specific conjugation of antibodies with cytotoxins to obtain stoichiometrically defined payload numbers and ADC preparations with defined DARs are possible but challenging [5]. Alternative non-IgG scaffolds, such as DARPins, are promising for tumor targeting due to their favorable biophysical properties even as fusions and conjugates, and they thus offer a large freedom of engineering [8]. For instance, the DARPin scaffold allows site-directed engineering of reactive groups almost anywhere in the sequence for well-defined conjugation reactions and fusion of effector domains to the N- and/or C-termini [9,10], as there are no interfering cysteines or disulfide bonds in the protein molecule.

Here we used the recently described DARPin fusion proteins with unstructured polypeptides [12] and introduced a single C-terminal

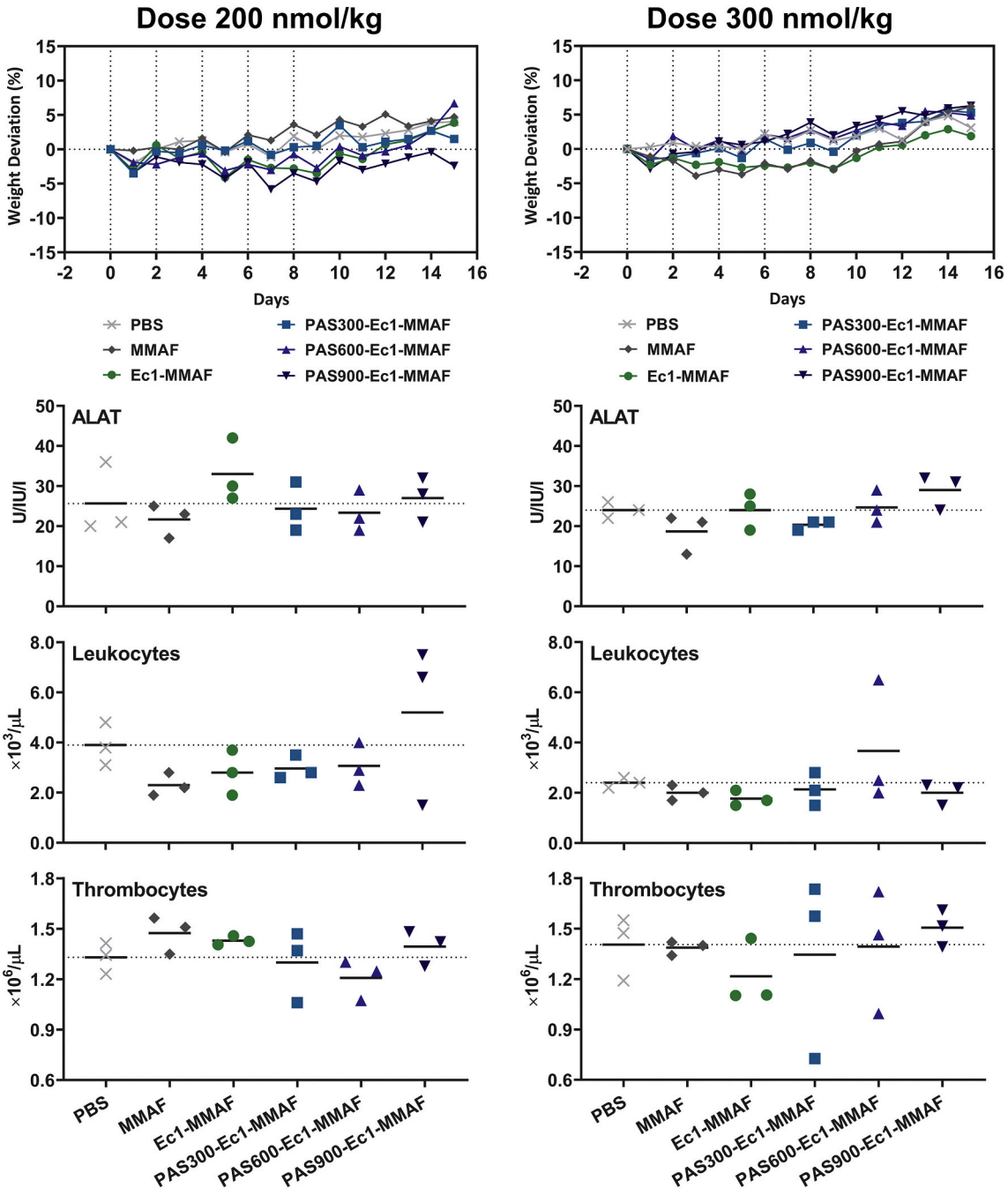

Fig. 3. Tolerability of free MMAF, Ec1-MMAF and PAS-Ec1-MMAF conjugates in CD-1 nude mice. The conjugates were injected every other day for five times and the body weight was monitored daily. One week after the last injection, mice were euthanized and the blood was analyzed for levels of alanine aminotransferase activity (ALAT), leukocytes and thrombocytes. For each group, 3 mice were analyzed.

cysteine for facile conjugation of the cytotoxin MMAF with thiol-maleimide chemistry [10,30] to generate a series of molecules with a range of molecular properties for systematic and comparative studies. As expected from previous results, the introduction of this conjugation site did not alter fundamental properties of the fusion proteins, such as expression, stability and cell binding, and resulted in homogeneous products with a defined 1:1 protein-to-drug ratio. The C-terminal MMAF with the maleimidocaproyl-linker adds an additional negative charge and increases the overall hydrophobicity of the otherwise hydrophilic fusion proteins. This feature of the polypeptide-DARPin-MMAF conjugates enabled us to prepare highly pure and molecularly defined products, either by anion exchange chromatography (AEX) or hydrophobic interaction chromatography (HIC). Sample preparation for HIC purification requires addition of high concentrations of ammonium sulfate to the protein samples, which leads to non-specific adsorption to plastic and thus loss of large quantities of protein. Therefore, AEX was better suited for large-scale purification (70–100 mg) of mono-conjugated products.

The purity of all preparations was > 95%. Electrospray ionization mass spectroscopy (ESI-MS) also confirmed the correct target masses, and that the samples consisted exclusively of the desired products, emphasizing the high purity of the mono-conjugates (Fig. 1C, Fig. S7, Table 1, Table S1). Surface plasmon resonance (SPR) also showed that conjugation of MMAF to the DARPin or the polypeptide-DARPin fusion proteins [12] did not affect binding affinity (Table 1, Table S1, Fig. S8). This high degree of product quality enabled us to investigate how

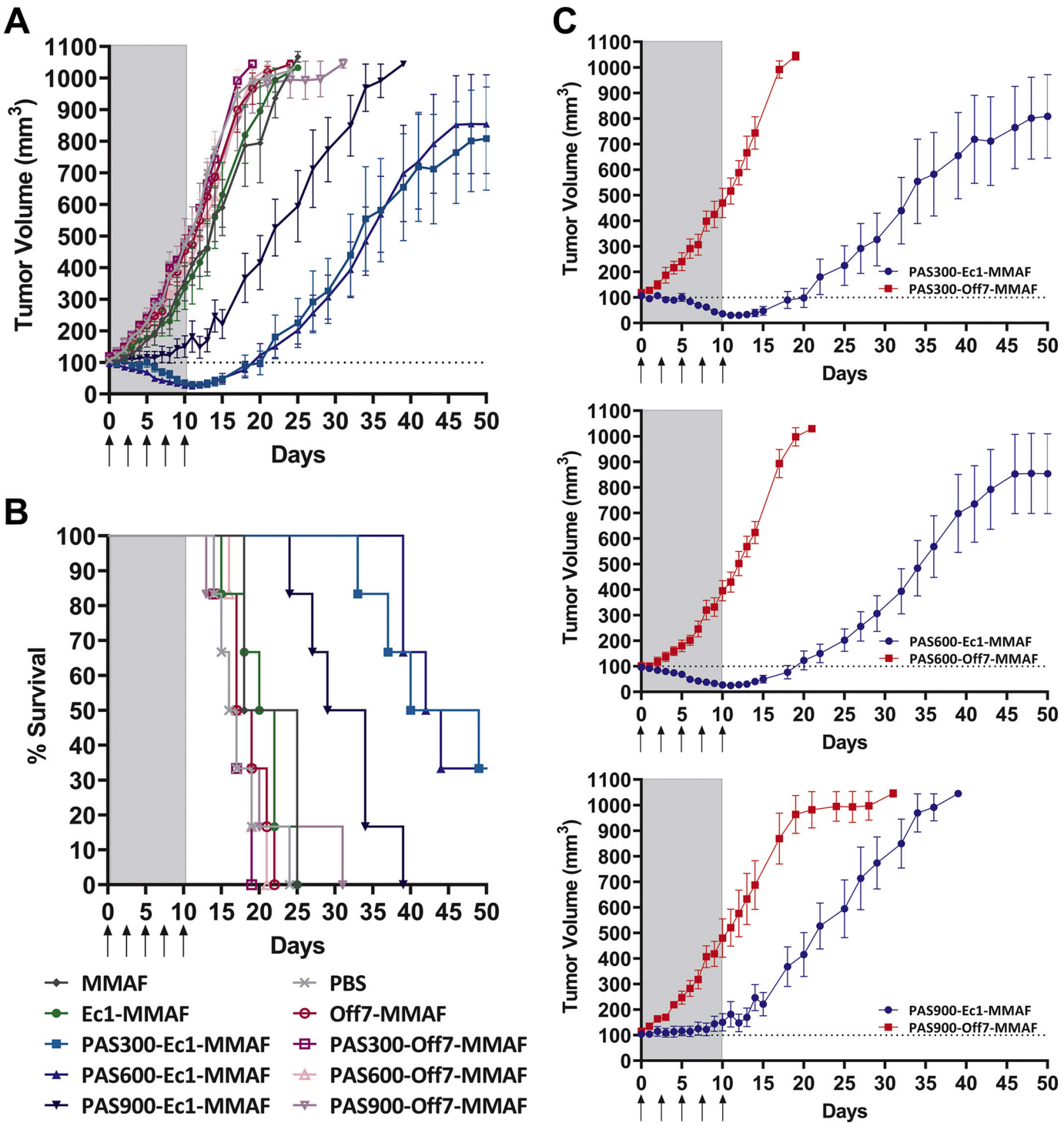

Fig. 4. Anti-tumor efficacy of the DARPin-MMAF and PAS-DARPin-MMAF conjugates in CD-1 nude mice. Mice (N = 6 mice per group) bearing EpCAM-positive HT29 tumor xenografts were injected every other day for five times with equimolar doses of 300 nmol/kg free MMAF, Ec1-MMAF, Off7-MMAF, and the PASylated conjugates or with 150 µL PBS as vehicle control. Arrows indicate days of injection. Tumor growth was monitored by caliper measurement during the course of 50 days. Data points represent the mean tumor volume ± SEM of 6 mice. A) Tumor growth curves of all treatment groups, B) Kaplan-Meier survival plot with an endpoint defined as a tumor volume of 1000 mm^3. C) Comparison of the tumor growth curves from mice treated with the size-matched EpCAM-targeting PAS-Ec1-MMAF and non-targeting control PAS-Off7-MMAF.

apparent molecular size affects half-life, tolerability, and anti-tumor efficacy.

4.2. Cytotoxicity is in the low nM range and independent of polypeptide length and type

As shown for antibody-MMAF [30] and DARPin-MMAF conjugates [10], upon internalization and lysosomal degradation, the cysteine-linked MMAF adduct is released into the cytosol to induce G2/M-phase arrest and apoptosis [33–35]. Here, we demonstrated EpCAM-specific killing of tumor target cells in the low nM range for all Ec1 DARPin-MMAF conjugates, independent of size, polypeptide type (XTEN or PAS) and length (XTEN288/PAS300, XTEN576/PAS600, XTEN864/PAS900) (Fig. 2, Table 2, Fig. S9, Table S2). On the other hand, all non-targeting conjugates with control DARPin Off7 showed much lower cytotoxicity, which was also independent of EpCAM (Table 2, Table S2). As expected, free MMAF was also less potent, due to its negative charge, which decreases membrane permeability and reduces internalization by pinocytosis.

The high potency and specificity of the EpCAM-targeting conjugates holds promise for better efficacy and tolerability *in vivo,* particularly for the polypeptide conjugates with high tumor localization and little non-specific accumulation in off-target tissues [12], as it will allow higher and repeated dosing.

4.3. Mice tolerate repeated injection of 300 nmol/kg PAS-DARPin-MMAF

Although the PASylated and XTENylated conjugates were equally potent *in vitro*, we focused on PAS-DARPin-MMAF for *in vivo* evaluation of tolerability and anti-tumor efficacy for several reasons. The PAS-DARPin-MMAF conjugates can be more easily produced at high yield and obtained in high purity by AEX, because the PAS-polypeptide lacks a negative charge, unlike XTEN, and the additional charge of MMAF can thus be used for separation of conjugate from non-conjugate.

Systemic administration of cytotoxins is commonly associated with unwanted side-effects due to off-target toxicity to vital non-tumor tissues [36], and this increases with increasing circulation time and dose. If toxicity increases more strongly than efficacy with molecular weight, this will narrow the therapeutic window. A few ADCs with MMAF have been approved for oncology indications due to their promising efficacy-to-tolerability profile [2,37]. Common side effects include thrombocytopenia, leukocytopenia and elevation of liver enzymes (ALAT, ASAT), all of which can be easily monitored in mice [38]. In mice, a maximum-tolerated dose of > 16 mg/kg (21 μmol/kg) free MMAF was determined [30], and in the same study an ADC with a drug-to-antibody ratio of 4.0 was well tolerated at doses > 150 mg/kg (approx. 1 μmol/kg). Here, we used repeated dosing of 300 nmol/kg free MMAF, DARPin-MMAF and polypeptide-DARPin-MMAF conjugates injected every other day for five times, without observing changes in body weight or blood parameters (Fig. 3, Fig. S11).

4.4. The anti-tumor efficacy of PAS-DARPin-MMAF conjugates has a molecular size optimum when injected in equimolar doses

Using HT29 tumor xenografts in nude mice we systematically investigated the anti-tumor efficacy and tolerability of the MMAF conjugates of different sizes and serum half-lives, to investigate whether the benefit is simply proportional to half-life or whether there is an optimum.

We found that the small size formats (free MMAF and DARPin-MMAF) had no anti-tumor efficacy (Fig. 4A, Fig. S12). In contrast, tumor control was achieved with all PASylated, half-life-extended conjugates (Fig. 4A,C). Importantly, the medium size conjugates PAS300-Ec1-MMAF and PAS600-Ec1-MMAF showed clearly more pronounced effects than the larger PAS900-Ec1-MMAF.

Various factors related to size are known to affect tumor targeting with drug conjugates. On the systemic level, they comprise extravasation, intratumoral distribution and tissue penetration, and excretion rate, which is the main factor influencing serum half-life. Cell binding affinity is linked to a phenomenon often called “binding-site barrier”, an observation that tight binding proteins will fully occupy the receptors, starting from the outside of the tumor and not reaching the inside. The suggestive name does not necessarily imply a physical barrier of the leading molecules for the molecules that follow [39,40]. On the cellular level, the rate of internalization and processing to release active drug [41,42] may also be related to molecular size parameters, and could thus potentially be rate-limiting and influence the efficacy on cells expressing the target. On the other hand, we could rule out affinity as a relevant parameter, as all constructs had essentially the same affinity.

Thus, treatment success depends on a complex relationship of these factors with size. For example, large size prolongs half-life and thus creates a depot-effect of the circulation but, on the other hand, impairs extravasation and tissue penetration. Nonetheless, cellular effects were found to show no size dependence: the toxicity as a function of time was essentially the same for all PASylated constructs, independent of size (Fig. S10).

Since clearly an optimum was found for efficacy in tumor control for the PASylated constructs of intermediate size (Fig. 4), as the efficacy decreased again with the longest PAS900 construct, we have to consider explanations within the systemic effect, and not reasons involving cellular kinetics or molecular interactions.

4.5. Localization and extravasation

Although, in principle, MMAF and DARPin-MMAF conjugates are small enough to uniformly distribute in the xenografts, they have too a short half-live, due to rapid renal excretion, which impairs tumor targeting [10]. Therefore, the overall level in the tumor is too low to control tumor growth (Fig. 4).

For the EpCAM-targeting PAS-DARPin fusion proteins tumor localization increases with molecular size and was indeed highest for the PAS900 conjugate [12]. The reason why the PAS300 or PAS600 conjugates controlled tumor growth better than the PAS900 conjugate can thus not be explained by the overall tumor localization, but it is possible that upon extravasation more of the large conjugate is trapped in the perivascular space [43].

The extravasation rate depends on the fenestration of the vascular endothelium in the tumor [44–46]. A recent study demonstrated that the blood vessels in HT29 tumor xenografts in mice are well fenestrated: a branched PEG40K conjugate with a molecular diameter of about 15 nm showed significantly higher tumor localization than nanoparticles > 150 nm [47], indicating less hindered extravasation for molecules in this size range. This finding is also confirmed by mathematical modeling and simulation data [45]. Differences in the extravasation rate of the PAS-DARPin-MMAF conjugates are therefore likely to be only small, due to their comparatively small size with diameters of 8 to 15 nm [12], which is below the pore size assumed for the fenestrated tumor vasculature [44,45,48].

4.6. Intratumoral diffusion

Upon extravasation, drug conjugates must evenly distribute in the tumor tissue to deliver the effector function to as many tumor cells as possible, and this process is dependent on the diffusion coefficient. While it is difficult to calculate a meaningful diffusion coefficient for a random flight polymer, such as PAS and XTEN, in dense tumor tissue, it is reasonable to assume that the diffusion coefficient will decrease with size [49,50]. This aspect is particularly important when MMAF is used as a cytotoxin, as it does not benefit from a bystander effect [30,51].

Studies with fluorescently labeled octyl chitosan nanocarriers in the range of 1 kDa to 300 kDa [43] and mathematical modeling and

simulation [21] are consistent with the expectation that intratumoral diffusion decreases with molecular size, even though the quantitative dependency for the random flight polymers is not clear. The modeling is also made difficult by inhomogeneous vascularization, mechanical obstacles by the stroma and interstitial pressure [39]. Depending on the degree of tortuosity and size of the conjugate, diffusion rates in tumors can drop to very low levels [52].

In summary, due to the effect of effective molecular weight on the diffusion coefficient, intratumoral distribution and penetration are slowed down, favoring an uneven distribution, which makes treatment success unlikely. Thus, there seems to be a critical size where tumor drug load and tissue penetration are optimally balanced.

4.7. Intra- and intermolecular blocking might enhance the effect of reduced diffusion coefficients

We previously described that modification of binding proteins with a bulky polymer such as PEG can alter the binding kinetics by slight reduction of the association rate constant (k_a), due to transient intramolecular blocking of the paratope [53]. In addition, the polymer can cause intermolecular blocking of the epitope by "diagonal parking" on the cell surface and thus decrease the maximal number of receptors that can be engaged at any time. While slightly reduced association rate constants (k_a) on EpCAM were measured for the polypeptide-DARPin fusion proteins [12] and here for the respective MMAF conjugates (Table 1, Table S1, Fig. S8), we conclude that these on-rate differences were irrelevant for intoxication (Fig. S10), since the cytotoxicity assay as a function of time showed no difference between the polymers of different length. Nonetheless, we cannot exclude that the effect of lower maximal loading ("diagonal parking") with increased size might negatively affect anti-tumor efficacy *in vivo*.

4.8. Perspectives

Since the molecular size has an optimum, an obvious measure to enhance efficacy would be to introduce additional cysteines in the polypeptide sequence, thereby increasing the number of conjugated drug molecules at a given size. In a similar approach, XTEN polypeptides were loaded with multiple anti-retroviral peptides in one molecule [54] and, comparing this to the naked anti-retroviral peptide T-20 itself, it was shown that this increases serum half-life and solubility of the fairly insoluble peptide. Because of the hydrophilicity of XTEN, and probably PAS, several MMAF molecules can be conjugated without hampering the favorable properties of the molecule (F. Brandl, S. Busslinger et al., unpublished). Because of the excellent tolerability of the drug conjugates tested here, it is likely that they are far away from the maximal tolerated dose and that the drug load could thus be increased.

5. Conclusions

We engineered a series of molecules which have exactly the same protein-to-drug ratio, the same attachment site and linker chemistry, the same epitope and affinity, and only differ by their effective molecular size. We also generated a series of matching controls that are identical in all aspects except that they do not bind to the tumor cells — to account for any enhanced permeability and retention (EPR) effect independent of the actual direct cellular targeting. Our results clearly show that for cytotoxic protein-drug conjugates engineered for tumor targeting there is a size window where the efficacy is optimal. We conclude that this is primarily an effect of the counterbalancing effect of intratumoral diffusion and serum half-life. The effect of extravasation is considered small in the tumor model chosen, and our measurements indicate that the effects of on-rate (and thus affinity) on the cytotoxicity and anti-tumor efficacy are essentially negligible, and the maximal receptor loading effects ("diagonal parking") do not influence toxicity conferred on tumor cells.

While the present study has highlighted these dependencies, it will still be necessary in the near future to determine the actual optimum experimentally in preclinical tumor models, and it will be a further challenge to properly scale this to the clinical setting. Nonetheless, this study has illuminated that, in a given tumor model with its intrinsic anatomical and physiological properties, next to drug and linker considerations, the actual pharmacokinetic and diffusion behavior of the protein-drug conjugate are of equal importance.

Acknowledgements

The authors would like to thank Hannes Merten for helpful discussions and advice, and Dr. Svende Pfundstein for help and advice with the in vivo studies. This work was supported by the Schweizerische Nationalfonds grant 31003A_170134.

Appendix A. Supplementary data

Supplementary data to this article can be found online at https://doi.org/10.1016/j.jconrel.2020.08.004.

References

[1] J.M. Lambert, A. Berkenblit, Antibody-drug conjugates for cancer treatment, Annu. Rev. Med. 69 (2018) 191–207.
[2] C.H. Chau, P.S. Steeg, W.D. Figg, Antibody-drug conjugates for cancer, Lancet 394 (2019) 793–804.
[3] G.M. Thurber, M.M. Schmidt, K.D. Wittrup, Antibody tumor penetration: transport opposed by systemic and antigen-mediated clearance, Adv. Drug Deliv. Rev. 60 (2008) 1421–1434.
[4] H.W. Schroeder Jr., L. Cavacini, Structure and function of immunoglobulins, J. Allergy Clin. Immunol. 125 (2010) S41–S52.
[5] H. Merten, F. Brandl, A. Plückthun, U. Zangemeister-Wittke, Antibody-drug conjugates for tumor targeting - novel conjugation chemistries and the promise of non-IgG binding proteins, Bioconjug. Chem. 26 (2015) 2176–2185.
[6] M. Gebauer, A. Skerra, Engineered protein scaffolds as next-generation therapeutics, Annu. Rev. Pharmacol. Toxicol. 60 (2020) 391–415.
[7] R. Simeon, Z. Chen, In vitro-engineered non-antibody protein therapeutics, Protein Cell 9 (2018) 3–14.
[8] A. Plückthun, Designed ankyrin repeat proteins (DARPins): binding proteins for research, diagnostics, and therapy, Annu. Rev. Pharmacol. Toxicol. 55 (2015) 489–511.
[9] M. Simon, U. Zangemeister-Wittke, A. Plückthun, Facile double-functionalization of designed ankyrin repeat proteins using click and thiol chemistries, Bioconjug. Chem. 23 (2012) 279–286.
[10] M. Simon, R. Frey, U. Zangemeister-Wittke, A. Plückthun, Orthogonal assembly of a designed ankyrin repeat protein-cytotoxin conjugate with a clickable serum albumin module for half-life extension, Bioconjug. Chem. 24 (2013) 1955–1966.
[11] C. Zahnd, M. Kawe, M.T. Stumpp, C. de Pasquale, R. Tamaskovic, G. Nagy-Davidescu, B. Dreier, R. Schibli, H.K. Binz, R. Waibel, A. Plückthun, Efficient tumor targeting with high-affinity designed ankyrin repeat proteins: effects of affinity and molecular size, Cancer Res. 70 (2010) 1595–1605.
[12] F. Brandl, H. Merten, M. Zimmermann, M. Béhé, U. Zangemeister-Wittke, A. Plückthun, Influence of size and charge of unstructured polypeptides on pharmacokinetics and biodistribution of targeted fusion proteins, J. Control. Release 307 (2019) 379–392.
[13] R. Jafari, N.M. Zolbanin, H. Rafatpanah, J. Majidi, T. Kazemi, Fc-fusion proteins in therapy: an updated view, Curr. Med. Chem. 24 (2017) 1228–1237.
[14] D. Sleep, J. Cameron, L.R. Evans, Albumin as a versatile platform for drug half-life extension, Biochim. Biophys. Acta 1830 (2013) 5526–5534.
[15] C. Cantante, S. Lourenço, M. Morais, J. Leandro, L. Gano, N. Silva, P. Leandro, M. Serrano, A.O. Henriques, A. Andre, C. Cunha-Santos, C. Fontes, J.D.G. Correia, F. Aires-da-Silva, J. Goncalves, Albumin-binding domain from *Streptococcus zooepidemicus* protein Zag as a novel strategy to improve the half-life of therapeutic proteins, J. Biotechnol. 253 (2017) 23–33.
[16] D. Steiner, F.W. Merz, I. Sonderegger, M. Gulotti-Georgieva, D. Villemagne, D.J. Phillips, P. Forrer, M.T. Stumpp, C. Zitt, H.K. Binz, Half-life extension using serum albumin-binding DARPin® domains, Protein Eng. Des. Sel. 30 (2017) 583–591.
[17] M. Schlapschy, U. Binder, C. Börger, I. Theobald, K. Wachinger, S. Kisling, D. Haller, A. Skerra, PASylation: a biological alternative to PEGylation for extending the plasma half-life of pharmaceutically active proteins, Protein Eng. Des. Sel. 26 (2013) 489–501.
[18] V. Schellenberger, C.W. Wang, N.C. Geething, B.J. Spink, A. Campbell, W. To, M.D. Scholle, Y. Yin, Y. Yao, O. Bogin, J.L. Cleland, J. Silverman, W.P. Stemmer, A recombinant polypeptide extends the in vivo half-life of peptides and proteins in a tunable manner, Nat. Biotechnol. 27 (2009) 1186–1190.

[19] R. Sutherland, F. Buchegger, M. Schreyer, A. Vacca, J.P. Mach, Penetration and binding of radiolabeled anti-carcinoembryonic antigen monoclonal antibodies and their antigen binding fragments in human colon multicellular tumor spheroids, Cancer Res. 47 (1987) 1627–1633.
[20] R. Muchekehu, D. Liu, M. Horn, L. Campbell, J. Del Rosario, M. Bacica, H. Moskowitz, T. Osothprarop, A. Dirksen, V. Doppalapudi, A. Kaspar, S.R. Pirie-Shepherd, J. Coronella, The effect of molecular weight, PK, and valency on tumor biodistribution and efficacy of antibody-based drugs, Transl. Oncol. 6 (2013) 562–572.
[21] M.M. Schmidt, K.D. Wittrup, A modeling analysis of the effects of molecular size and binding affinity on tumor targeting, Mol. Cancer Ther. 8 (2009) 2861–2871.
[22] M.R. Dreher, W. Liu, C.R. Michelich, M.W. Dewhirst, F. Yuan, A. Chilkoti, Tumor vascular permeability, accumulation, and penetration of macromolecular drug carriers, J. Natl. Cancer Inst. 98 (2006) 335–344.
[23] N. Stefan, P. Martin-Killias, S. Wyss-Stoeckle, A. Honegger, U. Zangemeister-Wittke, A. Plückthun, DARPins recognizing the tumor-associated antigen EpCAM selected by phage and ribosome display and engineered for multivalency, J. Mol. Biol. 413 (2011) 826–843.
[24] J.D. Pedelacq, S. Cabantous, T. Tran, T.C. Terwilliger, G.S. Waldo, Engineering and characterization of a superfolder green fluorescent protein, Nat. Biotechnol. 24 (2006) 79–88.
[25] H.K. Binz, P. Amstutz, A. Kohl, M.T. Stumpp, C. Briand, P. Forrer, M.G. Grütter, A. Plückthun, High-affinity binders selected from designed ankyrin repeat protein libraries, Nat. Biotechnol. 22 (2004) 575–582.
[26] F.W. Studier, Stable expression clones and auto-induction for protein production in *E. coli*, Methods Mol. Biol. 1091 (2014) 17–32.
[27] S. Hansen, J.C. Stüber, P. Ernst, A. Koch, D. Bojar, A. Batyuk, A. Plückthun, Design and applications of a clamp for green fluorescent protein with picomolar affinity, Sci. Rep. 7 (2017) 16292.
[28] J.E. Tropea, S. Cherry, D.S. Waugh, Expression and purification of soluble his(6)-tagged TEV protease, Methods Mol. Biol. 498 (2009) 297–307.
[29] P. Martin-Killias, N. Stefan, S. Rothschild, A. Plückthun, U. Zangemeister-Wittke, A novel fusion toxin derived from an EpCAM-specific designed ankyrin repeat protein has potent antitumor activity, Clin. Cancer Res. 17 (2011) 100–110.
[30] S.O. Doronina, B.A. Mendelsohn, T.D. Bovee, C.G. Cerveny, S.C. Alley, D.L. Meyer, E. Oflazoglu, B.E. Toki, R.J. Sanderson, R.F. Zabinski, A.F. Wahl, P.D. Senter, Enhanced activity of monomethylauristatin F through monoclonal antibody delivery: effects of linker technology on efficacy and toxicity, Bioconjug. Chem. 17 (2006) 114–124.
[31] V. Tolmachev, C. Hofström, J. Malmberg, S. Ahlgren, S.J. Hosseinimehr, M. Sandström, L. Abrahmsen, A. Orlova, T. Gräslund, HEHEHE-tagged affibody molecule may be purified by IMAC, is conveniently labeled with $[^{99m}Tc(CO)_3]^+$, and shows improved biodistribution with reduced hepatic radioactivity accumulation, Bioconjug. Chem. 21 (2010) 2013–2022.
[32] C. Hofström, M. Altai, H. Honarvar, J. Strand, J. Malmberg, S.J. Hosseinimehr, A. Orlova, T. Gräslund, V. Tolmachev, HAHAHA, HEHEHE, HIHIHI, or HKHKHK: influence of position and composition of histidine containing tags on biodistribution of $[^{99m}Tc(CO)_3]^+$-labeled affibody molecules, J. Med. Chem. 56 (2013) 4966–4974.
[33] J.A. Francisco, C.G. Cerveny, D.L. Meyer, B.J. Mixan, K. Klussman, D.F. Chace, S.X. Rejniak, K.A. Gordon, R. DeBlanc, B.E. Toki, C.L. Law, S.O. Doronina, C.B. Siegall, P.D. Senter, A.F. Wahl, cAC10-vcMMAE, an anti-CD30-monomethyl auristatin E conjugate with potent and selective antitumor activity, Blood 102 (2003) 1458–1465.
[34] N. Nilchan, X. Li, L. Pedzisa, A.R. Nanna, W.R. Roush, C. Rader, Dual-mechanistic antibody-drug conjugate via site-specific selenocysteine/cysteine conjugation, Antib. Ther. 2 (2019) 71–78.
[35] A.B. Waight, K. Bargsten, S. Doronina, M.O. Steinmetz, D. Sussman, A.E. Prota, Structural basis of microtubule destabilization by potent auristatin anti-mitotics, PLoS One 11 (2016) e0160890.
[36] D.G. Rudmann, On-target and off-target-based toxicologic effects, Toxicol. Pathol. 41 (2013) 310–314.
[37] H. Donaghy, Effects of antibody, drug and linker on the preclinical and clinical toxicities of antibody-drug conjugates, MAbs 8 (2016) 659–671.
[38] M.J. Hinrichs, R. Dixit, Antibody drug conjugates: nonclinical safety considerations, AAPS J. 17 (2015) 1055–1064.
[39] V.P. Chauhan, R.K. Jain, Strategies for advancing cancer nanomedicine, Nat. Mater. 12 (2013) 958–962.
[40] C. Vasalou, G. Helmlinger, B. Gomes, A mechanistic tumor penetration model to guide antibody drug conjugate design, PLoS One 10 (2015) e0118977.
[41] K.F. Maass, C. Kulkarni, A.M. Betts, K.D. Wittrup, Determination of cellular processing rates for a trastuzumab-maytansinoid antibody-drug conjugate (ADC) highlights key parameters for ADC design, AAPS J. 18 (2016) 635–646.
[42] J.C. Stüber, F. Kast, A. Plückthun, High-throughput quantification of surface protein internalization and degradation, ACS Chem. Biol. 14 (2019) 1154–1163.
[43] M. Zhang, Y. Ma, Z. Wang, Z. Han, W. Gao, Y. Gu, Optimizing molecular weight of octyl chitosan as drug carrier for improving tumor therapeutic efficacy, Oncotarget 8 (2017) 64237–64249.
[44] S.K. Hobbs, W.L. Monsky, F. Yuan, W.G. Roberts, L. Griffith, V.P. Torchilin, R.K. Jain, Regulation of transport pathways in tumor vessels: role of tumor type and microenvironment, Proc. Natl. Acad. Sci. U. S. A. 95 (1998) 4607–4612.
[45] V.P. Chauhan, T. Stylianopoulos, J.D. Martin, Z. Popovic, O. Chen, W.S. Kamoun, M.G. Bawendi, D. Fukumura, R.K. Jain, Normalization of tumour blood vessels improves the delivery of nanomedicines in a size-dependent manner, Nat. Nanotechnol. 7 (2012) 383–388.
[46] F. Yuan, M. Dellian, D. Fukumura, M. Leunig, D.A. Berk, V.P. Torchilin, R.K. Jain, Vascular permeability in a human tumor xenograft: molecular size dependence and cutoff size, Cancer Res. 55 (1995) 3752–3756.
[47] D.R. Beckford Vera, S.D. Fontaine, H.F. VanBrocklin, B.R. Hearn, R. Reid, G.W. Ashley, D.V. Santi, PET imaging of the EPR effect in tumor xenografts using small 15 nm diameter polyethylene glycols labeled with zirconium-89, Mol. Cancer Ther. 19 (2020) 673–679.
[48] T. Stylianopoulos, R.K. Jain, Design considerations for nanotherapeutics in oncology, Nanomedicine 11 (2015) 1893–1907.
[49] L.J. Nugent, R.K. Jain, Extravascular diffusion in normal and neoplastic tissues, Cancer Res. 44 (1984) 238–244.
[50] G.M. Thurber, M.M. Schmidt, K.D. Wittrup, Factors determining antibody distribution in tumors, Trends Pharmacol. Sci. 29 (2008) 57–61.
[51] M.S. Sutherland, R.J. Sanderson, K.A. Gordon, J. Andreyka, C.G. Cerveny, C. Yu, T.S. Lewis, D.L. Meyer, R.F. Zabinski, S.O. Doronina, P.D. Senter, C.L. Law, A.F. Wahl, Lysosomal trafficking and cysteine protease metabolism confer target-specific cytotoxicity by peptide-linked anti-CD30-auristatin conjugates, J. Biol. Chem. 281 (2006) 10540–10547.
[52] A. Pluen, Y. Boucher, S. Ramanujan, T.D. McKee, T. Gohongi, E. di Tomaso, E.B. Brown, Y. Izumi, R.B. Campbell, D.A. Berk, R.K. Jain, Role of tumor-host interactions in interstitial diffusion of macromolecules: cranial vs. subcutaneous tumors, Proc. Natl. Acad. Sci. U. S. A. 98 (2001) 4628–4633.
[53] S. Kubetzko, C.A. Sarkar, A. Plückthun, Protein PEGylation decreases observed target association rates via a dual blocking mechanism, Mol. Pharmacol. 68 (2005) 1439–1454.
[54] S. Ding, M. Song, B.C. Sim, C. Gu, V.N. Podust, C.W. Wang, B. McLaughlin, T.P. Shah, R. Lax, R. Gast, R. Sharan, A. Vasek, M.A. Hartman, C. Deniston, P. Srinivas, V. Schellenberger, Multivalent antiviral XTEN-peptide conjugates with long in vivo half-life and enhanced solubility, Bioconjug. Chem. 25 (2014) 1351–1359.